Time-dependent wave-packet method for the complete determination of S-matrix elements for reactive molecular collisions in three dimensions

Richard S. Judson and Donald J. Kouri
Department of Chemistry and Department of Physics, University of Houston, Houston, Texas 77204-5641

Daniel Neuhauser and Michael Baer
Department of Applied Mathematics, Soreq Nuclear Research Center, Yavne 70600, Israel
(Received 6 November 1989)

An alternative time-dependent wave-packet method for treating three-dimensional gas phase reactive atom-diatom collisions is presented. The method employs a nonreactive body-frame wave-packet propagation procedure, made possible by judicious use of absorbing optical potentials, a novel scheme for interpolating the wave function from coordinates in one arrangement to those in another and the fact that the time-dependent Schrödinger equation is an initial-value problem. The last feature makes possible a computationally viable and accurate procedure for changing from one arrangement's coordinates to another. In addition, the method allows the determination of S-matrix elements over a wide range of energies from a single wave-packet propagation. The determination of scattering into any particular arrangement is effectively decoupled from that into other arrangements by means of complex absorbing potentials. The method is illustrated by carrying out detailed calculations of inelastic and reactive scattering in the $H+H_2$ system using the Liu-Siegbahn-Truhlar-Horowitz potential surface.

I. INTRODUCTION

Much effort has been expended over the last several years to develop methods for performing molecular-scattering calculations that exploit the powerful capabilities of the present generation of supercomputers. The majority of this work has concentrated on developing efficient algorithms for solving the time-independent Schrödinger equation.[1-11] The time-independent algorithms have been (and continue to be) highly refined to take full advantage of the large, high-speed core memory and vectorizing capabilities of supercomputers such as the Cray. The root of the efficiency of these algorithms is that they reduce the solution of the Schrödinger equation to a problem in linear algebra, for which many efficient solution methods exist. However, the *noniterative*, time-independent, matrix formulations that are commonly used have an inherent problem, namely, the fact that for sufficiently large problems (meaning those that require large numbers of basis functions for a full description of the system), the cost of obtaining the solution increases approximately as the cube of the size of the algebraic equations or coupled equations. Due to this rapid scaling with problem size, even the most efficient of the currently existing noniterative, time-independent algorithms stretch the limits of the largest available computers, for even moderate-sized problems.

Over the years, a substantial amount of effort has been invested in solving the time-dependent Schrödinger equation[12-32] and recently it has been recognized that the time-dependent formulation provides one way around the N^3 scaling dilemma inherent in noniterative, time-independent scattering formulations. This is due to the initial-value nature of the time-dependent formulation, which allows methods that scale as N^2 or slower, where N is the number of internal states needed to describe the system. (Note that it is also possible to use time-independent iterative methods to circumvent this problem.[33] This leads to methods scaling as N^2.) Several promising time-dependent three-dimensional (3D) gas phase methods have been developed.[21,23,27,30-32] We have numerically tested one method for performing atom-rigid rotor-scattering calculations that scale as $N^{3/2}$ in the limit of large N.[27] The scaling factor can be reduced further to $N \log_2 N$ with appropriate modifications. In order for the time-dependent (TD) methods to be competitive with the time-independent (TI) techniques, two criteria must be met. First, the relatively slow scaling of the TD method must be manifested for small enough problems that it becomes a practical advantage. Second, the TD method must be capable of providing as much detailed information as the TI methods. In particular, a TD method should be able to generate a complete column of the S matrix for a range of energies for a reactive collision system. In this paper we report a new TD method that meets both of these criteria—namely, it produces a complete column of the reactive S matrix and does so efficiently. It also provides the corresponding inelastic S-matrix elements.

Wave-packet methods also have a number of conceptual advantages that give them an appeal over and above that of their efficiency. Most obviously, because reactions really happen in the time domain, watching the evolution of a wave packet can be a great aid in helping us understand the physics of the collision. Additionally, wave-packet calculations can be made to correspond to a

molecular-beam experiment where molecules in a few initial internal states are allowed to collide. In contrast, a noniterative, time-independent calculation provides information on all initial conditions, most of which are experimentally uninteresting for simulating molecular beams formed by supersonic nozzle techniques.

A TD computational scheme for performing reactive scattering calculations can be broken down into several stages. (1) The initial wave function in the initial asymptotic configuration $\psi(t=t_0)$ must be prescribed; (2) it must be propagated into the interaction region and back out again, yielding $\psi(t=t_f)$; and (3) the final wave packet must be analyzed to extract S-matrix elements in each of the energetically accessible arrangement configurations. The first step, prescription of the initial wave packet, is straightforward and somewhat arbitrary. Step (2), the propagation of the wave packet, is the source of most of the computational cost and must be done as efficiently as possible. A very efficient method has been developed by Kosloff and co-workers.[18] In their method, the wave function at time t_f is written as

$$\psi(t_f)=\exp[-iH(t_f-t_0)/\hbar]\psi(t_0) ,$$

where H is the full Hamiltonian operator. The propagator

$$\exp[-iH(t_f-t_0)/\hbar]$$

is approximated as a sum of Chebyshev polynomials, yielding a propagation scheme that is unitary and of high global accuracy. By combining the Chebyshev scheme with the fast Fourier transform (FFT) method[18] for calculating the action of the derivative operators in H, one obtains a general and efficient propagation scheme. For an atom-diatom system, the efficiency can be increased by using a body-frame coordinate representation.[27,30,32,34–39] The third step of the calculation, the problem of extracting the S matrix from $\psi(t_f)$ in all arrangements has until now been unsolved. There are two facets of the problem. First, the methods currently used for calculating S-matrix elements from the wave packet require knowing the value of the wave function at all points in each asymptotic arrangement. For an atom-diatom system, one straightforward way to get this information is to represent the wave function as $\psi(R_{AB},R_{BC},R_{CA},t)$, where R_{ij} is the distance between atoms i and j. This function is propagated until there is no probability for all three atoms being close together and then the final analysis is carried out. However, the representation of this function would require a three-dimensional array with each of the dimensions extending from very small to very large distances. Such an array would be prohibitively large to store and manipulate. A partial solution to the "representation-size" problem has recently been tested.[30–32] It is based on the observation that certain state-to-state transitions are substantially complete long before the wave function has reached the asymptotic region. In particular, if one analyzes the wave function for scattered fluxes just on the reactive product side of the interaction region, it is possible to calculate converged vibrationally resolved probabilities (though not S-matrix elements). Moving the analysis point further out would also allow the calculation of rotationally and vibrationally resolved probabilities. Once the fluxes are computed, the reactive wave is absorbed by means of a complex potential so that it need not be propagated further.[28–32] This method reduces the propagation region from the full (R_{AB},R_{BC},R_{CA}) space to the region needed to describe the initial asymptotic arrangement plus a relatively small extension in the directions of the reactive asymptotic arrangements. As reported, this method was relatively inefficient because it required packets narrow in momentum space and so a separate propagation was required for each energy. This particular problem is not fundamental to the method and has been overcome.[32] However, phase information is lost, which can be a drawback (e.g., if one desires differential cross sections).

In this paper we present an alternate scheme for circumventing the representation-size problem, while still allowing the calculation of individual S-matrix elements. We choose the initial wave packet to be narrow enough in configuration space that over some period in time it can be localized in the strong interaction region (all R's small). Our method uses the fact that knowledge of the wave function expressed in the coordinates appropriate to the initial inelastic arrangement (in which the incoming propagation was carried out) can be used to determine the wave function expressed in the coordinates appropriate to any other arrangement. In particular, we can take the function $\psi(R_\alpha,r_\alpha,\gamma_\alpha,t_{\rm int})$, where α designates the initial arrangement and $t_{\rm int}$ the time when the wave packet is localized in the interaction region, and can calculate $\psi(R_\beta,r_\beta,\gamma_\beta,t_{\rm int})$, which is the same wave packet, but now represented in terms of the inelastic coordinates appropriate to the reactive arrangement β. The advantage of this approach is that instead of representing the wave function on a single three-dimensional grid with all three dimensions large, we represent it on three three-dimensional grids but where each of these has only one dimension that is large. Complex absorbing potentials are placed appropriately in the arrangements for which we do not desire the scattering information.[28–32] As a result, these grids are in practice found to be only slightly larger than those needed to perform purely nonreactive calculations. If the wave function at $t_{\rm int}$ is saved, one can calculate the scattering in each arrangement successively. We employ packets that are narrow in configuration space so that one computation yields scattering information at many energies.

Because the wave function expressed in terms of one arrangement's coordinates at a time t can be used to determine accurately the wave function in another arrangement's coordinates at the same time, we only need to carry out nonreactive wave-packet propagations, thus greatly simplifying the problem. Furthermore, this procedure avoids all of the problems encountered in earlier time-independent approaches to reactive scattering that required matching the wave function and its directional derivatives determined by nonreactive propagation methods in each of the arrangements.[37–39] The present success is directly due to the initial-value nature of the time-dependent approach, as opposed to the boundary-

value nature of time-independent methods. The initial-value nature of the time-dependent equations, combined with the present procedure involving purely nonreactive wave-packet propagations, also avoids difficulties with "nonlocal" operators when rearrangements occur and one uses Jacobi-type coordinates appropriate to each arrangement.[40]

This paper is arranged as follows: In Sec. II we present the theory for atom-diatom scattering in the body frame, in addition to techniques needed to transform the wave function from one arrangement representation to another. In Sec. III we describe the computational algorithm used to incorporate reaction. In Sec. IV we present the results of a numerical example, $H+H_2$ $(J=0)$. Section V gives a brief discussion.

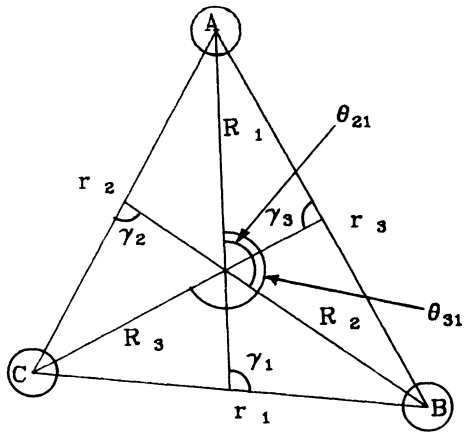

FIG. 1. An illustration of the coordinates used.

II. THEORY

In this section we present the equations needed for performing time-dependent scattering calculations for an atom-diatom system in three dimensions. In our scheme for performing *reactive* scattering calculations (described more fully in Sec. III), the wave function is always propagated and analyzed in terms of *inelastic* body-frame coordinates $(R_\alpha, r_\alpha, \gamma_\alpha)$ for arrangement α, where α can equal 1, 2, or 3. Here, r is the diatom internuclear separation, R is the distance from the atom to the diatom center of mass, and γ is the angle between $\hat{R}$ and $\hat{r}$. It is then necessary to have equations of motion, initial conditions, etc., known in terms of these inelastic arrangement coordinates. In Sec. II A we derive the body-frame equations of motion for the coupled-channel wave packets in a single arrangement. This is a direct extension of the atom-rigid rotor formalism presented earlier.[23,27] The form of the equations of motion is identical in all arrangements and, consequently, we will only label quantities by arrangement when confusion might otherwise arise. The convention we use for designating the arrangement number is arrangement 1 corresponds to $A+BC$, arrangement 2 corresponds to $B+CA$, and arrangement 3 corresponds to $C+AB$. These are illustrated in Fig. 1. In Sec. II B we prescribe appropriate initial conditions for the wave packets and in Sec. II C we describe how to form parity-conserving wave packets. The method for calculating S-matrix elements for any process from the wave packet at long times is described in Sec. II D.

This material is sufficient for performing calculations on nonreactive systems. Two additional items are needed to incorporate reaction. First, we need to be able to take the wave function expressed in terms of the inelastic coordinates appropriate to one arrangement and re-express it in terms of the inelastic coordinates appropriate to another. A new method for doing this is given in Sec. II E. Secondly, because the reactive portion of the wave packet will eventually move out of the region covered by the numerical nonreactive grid (and likewise the nonreactive portion will move out of the region described by the reactive grid), we must prevent it from reflecting unphysically off the grid boundary. In Sec. II F we describe the use of an optical potential[28–30] to absorb those portions of the wave packet that will move off the edge of a particular grid. This is a direct extension of the procedure presented earlier in methods for calculating vibrationally resolved reactive probabilities for collinear[28,29] and for three-dimensional[30–32] atom-diatom scattering problems.

A. Equations of motion

The physical wave packet for the $A+BC$ arrangement can be expanded in a body-fixed reference frame as[27,34–39]

$$\Psi(\hat{k}_0,n_0,j_0,m_0|\mathbf{R},\mathbf{r},t) = \frac{1}{rR}\sum_{J,j,\Omega}(2J+1)[D^J_{\Omega m_0}(\xi,\theta,\zeta)]^* Y_{j\Omega}(\gamma,0) \times \chi^J(j\Omega|n_0 j_0 m_0|R,r,t) \; . \tag{2.1}$$

Here, J is the total angular momentum quantum number, j is the diatomic rotational quantum number, Ω is the projection of j on the body-frame z axis (defined to be $\hat{R}$), n_0 and j_0 are the initial diatom vibrational and rotational quantum numbers, and m_0 is the initial projection of j and J on the space-fixed z axis. We have chosen the initial conditions so that at $t=0$, the relative momentum vector $\hat{k}$ is parallel to both the space-fixed and body-fixed z axes.[23,27] The factor $1/(rR)$ is included to simplify the equations of motion of the channel wave packets χ^J by eliminating all first derivative terms. The projection quantum number Ω ranges from $-\min(J,j)$ to $+\min(J,j)$. The function $[D^J_{\Omega m_0}(\xi,\theta,\zeta)]^*$ is a Wigner rotation matrix element[41] and $Y_{j\Omega}(\gamma,0)$ is a spherical harmonic. The total wave function obeys the time-dependent Schrödinger equation

$$i\hbar\frac{\partial}{\partial t}\Psi(\hat{k}_0,n_0,j_0,m_0|\mathbf{R},\mathbf{r},t) = H\Psi(\hat{k}_0,n_0,j_0,m_0|\mathbf{R},\mathbf{r},t) \; , \tag{2.2}$$

with the Hamiltonian being given by[34]

$$H=-\frac{\hbar^2}{2\mu}\frac{1}{R}\frac{\partial^2}{\partial R^2}R-\frac{\hbar^2}{2m}\frac{1}{r}\frac{\partial^2}{\partial r^2}r+\frac{\hbar^2}{2\mu R^2}l^2+\frac{\hbar^2}{2mr^2}\mathbf{j}^2+V(R,r,\gamma)\ , \tag{2.3}$$

where (in arrangement 1) $m=m_B m_C/(m_B+m_C)$ and

$$\mu=m_A(m_B+m_C)/(m_A+m_B+m_C)\ .$$

(The reduced masses m and μ must be changed appropriately in arrangements 2 and 3.) By substituting Eqs. (2.1) and (2.3) into Eq. (2.2) and projecting out the rotation matrices and spherical harmonics, we can arrive at a set of coupled equations for the channel wave packets,

$$i\hbar\frac{d}{dt}\chi^J(j'\Omega'|n_0j_0m_0|R,r,t)=\sum_{j\Omega}H^J(j'\Omega'|j\Omega)\chi^J(j\Omega|n_0j_0m_0|R,r,t)\ , \tag{2.4}$$

where the channel Hamiltonians are given by[27,34–39]

$$H^J(j'\Omega'|j\Omega)=\left[-\frac{\hbar^2}{2\mu}\frac{\partial^2}{\partial R^2}+\frac{\hbar^2}{2\mu R^2}[J(J+1)-2\Omega^2+j(j+1)]-\frac{\hbar^2}{2m}\frac{\partial^2}{\partial r^2}+\frac{\hbar^2}{2mr^2}j(j+1)+v(r)\right]\delta_{jj'}\delta_{\Omega\Omega'}$$
$$+V^{\Omega}(j'|j|R,r)\delta_{\Omega\Omega'}-\frac{\hbar^2}{2\mu R^2}[\lambda_+(J\Omega')\lambda_+(j\Omega')\delta_{\Omega'+1,\Omega}\delta_{jj'}+\lambda_-(J\Omega')\lambda_-(j\Omega')\delta_{\Omega'-1,\Omega}\delta_{jj'}] \tag{2.5}$$

and where

$$V^{\Omega}(j'|j|R,r)=2\pi\int_{-1}^{1}d(\cos\gamma)Y^*_{j\Omega}(\gamma,0)\times[V(R,r,\gamma)-v(r)]\times Y_{j'\Omega}(\gamma,0)\ , \tag{2.6}$$

$$v(r)=\lim_{R\to\infty}V(R,r,\gamma)\ , \tag{2.7}$$

$$\lambda_{\pm}(J\Omega)=[(J\pm\Omega+1)(J\mp\Omega)]^{1/2}\ . \tag{2.8}$$

The form of the body-frame Hamiltonian allows us to propagate the wave packets very efficiently. This is due to the kinetic energy being tridiagonal at worst and the potential being diagonal in Ω. Because the propagation in each arrangement is carried out in the appropriate inelastic coordinates, we retain these advantages even when we treat reaction. The wave packet is propagated using the Chebyshev method of Tal-Ezer and Kosloff,[18] as has been described elsewhere.[23] See Ref. 27 for details of applying the method to body-frame wave packets. The principal difference encountered when vibration is added is that we must calculate the action of the kinetic-energy operator in both non-Cartesian variables R and r. These operations are performed as before using fast Fourier transforms.[18,19] The FFT procedure used for the radial variables is that developed in Ref. 23. See Ref. 27 for a more complete discussion of the body-frame treatment and its scaling behavior with problem size. (Note that the equations of motion that include vibration in a space-frame treatment, which enter in the same way into the body-frame equations, were reported earlier, but were not tested numerically[23]).

B. Initial conditions

It is important, both for efficiency of propagation and for the method we use to incorporate reaction, that each of the wave-packet components

$$\chi^J(j\Omega|n_0j_0m_0|R,r,t)$$

be well localized throughout the propagation. Functions that satisfy this criterion are given by[27]

$$\chi^J(j\Omega|n_0j_0m_0|R,r,t=0)=\varphi_{n_0j_0}(r)\int_0^{\infty}dk_0\,A(k_0)\mathscr{J}^{Jj_0}_{\Omega m_0}(k_0R)\delta_{jj_0}\ , \tag{2.9}$$

where the $\varphi_{nj}(r)$ are eigenfunctions of the asymptotic diatom Hamiltonian

$$\left[-\frac{\hbar^2}{2m}\frac{\partial^2}{\partial r^2}+\frac{\hbar^2}{2mr^2}j(j+1)+v(r)\right]\varphi_{nj}(r)=\epsilon_{nj}\varphi_{nj}(r) \tag{2.10}$$

and $\mathscr{J}^{Jj_0}_{\Omega m_0}(k_0R)$ is a body-frame Bessel function[27,35,36] that is the radial part of the eigenfunction of the free Hamiltonian. We use the following definition which differs slightly from that given in Ref. 27:

$$\mathscr{J}^{Jj}_{mm'}(kR)=\left[\frac{2}{\pi}\right]^{1/2}kR\sum_l i^l(2l+1)(-1)^{m+m'}\times\begin{bmatrix}l & j & J\\ 0 & m & -m\end{bmatrix}\begin{bmatrix}l & j & J\\ 0 & m' & m'\end{bmatrix}\times j_l(kR)\ , \tag{2.11}$$

where $j_l(kR)$ is a spherical Ricatti-Bessel function[42] of order l and the terms

$$\begin{bmatrix}l & j & J\\ 0 & m' & -m'\end{bmatrix} \tag{2.12}$$

are $3-j$ symbols.[41] The stable Hankel transform method given in Ref. 23 is used when performing the integral in Eq. (2.9) and the equivalent ones that arise in the final-state analysis. The $\mathscr{J}^{Jj}_{mm'}(kR)$ obey the orthogonality and completeness relationship

$$\sum_{\Omega}\int_0^{\infty}dR\,[\mathscr{J}^{Jj}_{m\Omega}(kR)]^*\mathscr{J}^{Jj}_{\Omega m'}(k'R)=\delta(k-k')\delta_{mm'}\ . \tag{2.13}$$

Equation (2.9) shows that the initial wave packet is the product of a pure internal state times a superposition of translational states weighted by $A(k_0)$.

The function $A(k_0)$ in Eq. (2.9) gives the initial distribution in momentum or energy space. As previously,[27] we choose this function to be given by

$$A(k_0)=\int_0^\infty dR\, g(R)\mathcal{J}_{00}^{00}(k_0R)\ , \tag{2.14}$$

where $g(R)$ is a normalized Gaussian,

$$g(R)=R\frac{\pi}{2}[\sqrt{2\pi}\sigma(\sigma^2+R_0^2)]^{-1/2} \times\exp[-(R-R_0)^2/4\sigma^2-i\bar{k}_0R]\ . \tag{2.15}$$

R_0 is the location of the peak of the coordinate representation wave packet and σ is its width. The packet peaks in momentum space at $k_0=\bar{k}_0$, where

$$\bar{k}_0=\left[\left[\frac{2\mu}{\hbar^2}\right](E_0-\epsilon_{n_0j_0})-\frac{R_0^2}{4\sigma^2(\sigma^2+R_0^2)}\right]^{1/2}\ . \tag{2.16}$$

E_0 is the corresponding total energy at the peak of the momentum representation packet and $\epsilon_{n_0j_0}$ is the eigenenergy of the initial diatom state, defined in Eq. (2.10).

C. Symmetrization of the wave packet

Instead of propagating the full set of functions

$$\chi^J(j\Omega|n_0j_0m_0|R,r,t)$$

given in Eq. (2.4), we form linear combinations of these having definite parity. Parity is conserved both within and between arrangements so that functions of different parity can be propagated separately. The symmetrized functions are defined as

$$\chi_\pm^J(j\Omega|n_0j_0m_0|R,r,t) =\frac{1}{\sqrt{2}}[\chi^J(j\Omega|n_0j_0m_0|R,r,t) \pm\chi^J(j-\Omega|n_0j_0m_0|R,r,t)]\ . \tag{2.17}$$

The even and odd parity solutions obey the same set of equations as the original channel wave packets,[27] but with different initial conditions specified by Eq. (2.17). We only need to propagate the functions $\chi_\pm^J(j\Omega|n_0j_0m_0|R,r,t)$ for $\Omega\geq 0$. The corresponding functions for $\Omega<0$ are given by

$$\chi_\pm^J(j-\Omega|n_0j_0m_0|R,r,t)=\pm\chi_\pm^J(j\Omega|n_0j_0m_0|R,r,t)\ .$$

The complete solutions can be reformed using the formula

$$\chi^J(j\pm\Omega|n_0j_0m_0|R,r,t)=\frac{1}{\sqrt{2}}[\chi_+^J(j\Omega|n_0j_0m_0|R,r,t) \pm\chi_-^J(j\Omega|n_0j_0m_0|R,r,t)]\ . \tag{2.18}$$

D. Final-state analysis at long times

In this section we derive the formulas for calculating S-matrix elements from the wave packets in a given arrangement. This derivation closely follows the one given earlier for the rigid rotor case.[27] In the following analysis, the propagation is assumed to have started at a time t_0 when the wave packet was located well outside the interaction region. (In practice, t_0 is set to zero.) We assume that wave packets that are narrow in configuration space and hence broad in momentum space will be used, as in earlier work.[23,27] This enables us to obtain S-matrix elements over a wide range of energies from a single wave-packet propagation. For the analysis to be valid, the propagation must proceed to a time t_f when the probability density in the interaction region is once again vanishingly small. In particular, t_f must be longer than the lifetime of any resonance in the energy range significantly sampled by the wave packet. [See the discussion after Eq. (2.43) below for more information on this point.] In our derivation, the initial arrangement is denoted by α and the final arrangement by β, where β may or may not equal α. The derivation is given mainly in terms of abstract states parametrized by the energy E, and the results are later translated into the coordinate representation, parametrized by the wave number k. The derivation uses the complete wave packets rather than the parity-conserving linear combinations.

To begin, we denote the abstract eigenstates of the free Hamiltonian in arrangement β by $|\phi_{\beta njM}^J(E)\rangle$, i.e.,

$$(E-H_\beta)|\phi_{\beta njM}^J(E)\rangle=0\ , \tag{2.19}$$

where the total Hamiltonian H can be factored as

$$H=H_\beta+V_\beta\quad(\beta=1,2,3) \tag{2.20}$$

and where

$$H_\beta=\lim_{R_\beta\to\infty}H\ . \tag{2.21}$$

Therefore $V_\beta\equiv H-H_\beta$ and it follows that the perturbation V_β tends to zero as $R_\beta\to\infty$. In the mixed representation we are using, the free Hamiltonian eigenfunctions are given by

$$\langle[j'\Omega'R,r]_\beta|\phi_{\beta njM}^J(E)\rangle =\delta_{jj'}\left[\frac{\mu_\beta}{\hbar^2k}\right]^{1/2}\mathcal{J}_{\Omega\Omega'}^{Jj}(kR_\beta)\varphi_{nj}^\beta(r_\beta)\ , \tag{2.22}$$

where

$$E=\frac{\hbar^2k^2}{2\mu_\beta}+\epsilon_{nj}^\beta\ . \tag{2.23}$$

The asymptotic vibrational eigenfunctions $\varphi_{nj}^\beta(r_\beta)$ and eigenvalues ϵ_{nj}^β were defined in Eq. (2.10). This leads to the normalization [see Eq. (2.13)]

$$\langle\phi_{\beta njM}^J(E)|\phi_{\beta n'j'\Omega'}^J(E')\rangle=\delta_{nn'}\delta_{jj'}\delta_{\Omega\Omega'}\delta(E-E')\ . \tag{2.24}$$

To extract the long-time scattering information, we calculate the projection of the β arrangement free Hamil-

tonian eigenstate on the full wave packet that has propagated into the asymptotic region ($t \geq t_f$):

$$\tilde{I}^J_{\beta\alpha}(nj\Omega|n_0j_0m_0|E) = \lim_{t\geq t_f} \langle \phi^J_{\beta nj\Omega}(E)|\psi^J_{n_0j_0m_0}(t)\rangle \tag{2.25a}$$

$$= \lim_{t\geq t_f} \langle \phi^J_{\beta nj\Omega}(E)| \times \exp[-iH(t-t_0)/\hbar]|\psi^J_{n_0j_0m_0}(t_0)\rangle \tag{2.25b}$$

where $|\psi^J_{n_0j_0m_0}(t)\rangle$ is the time-dependent wave packet whose representation in arrangement β is

$$\langle [j\Omega Rr]_\beta|\psi^J_{n_0j_0m_0}(t)\rangle = \chi^J_\beta(j\Omega|n_0j_0m_0|R_\beta,r_\beta,t) , \tag{2.26}$$

where

$$\chi^J_\beta(j\Omega|n_0j_0m_0|R_\beta,r_\beta,t)$$

was defined in Eq. (2.1). The initial wave packet $|\psi^J_{n_0j_0m_0}(t_0)\rangle$ is given by [see Eq. (2.9)]

$$|\psi^J_{n_0j_0m_0}(t_0)\rangle = \int dE_0 \mathcal{A}(E_0)|\phi^J_{\alpha n_0j_0m_0}(E_0)\rangle . \tag{2.27}$$

If we substitute Eq. (2.27) into Eq. (2.25b), we arrive at

$$\tilde{I}^J_{\beta\alpha}(nj\Omega|n_0j_0m_0|E) = \lim_{t\geq t_f} \int dE_0 \mathcal{A}(E_0)\langle \phi^J_{\beta nj\Omega}(E)|\exp[-iH(t-t_0)/\hbar]|\phi^J_{\alpha n_0j_0m_0}(E_0)\rangle$$
$$= \lim_{t\geq t_f} \int dE_0 \mathcal{A}(E_0)\exp(-iEt/\hbar)\exp(iE_0t_0/\hbar)\langle \phi^J_{\beta nj\Omega}(E)|\hat{U}^{\beta\alpha}_I(t,t_0)|\phi^J_{\alpha n_0j_0m_0}(E_0)\rangle , \tag{2.28}$$

where $\hat{U}^{\beta\alpha}_I(t,t_0)$ is the time evolution operator in the interaction picture

$$\hat{U}^{\beta\alpha}_I(t,t_0) = \exp(iH_\beta t/\hbar)\exp[-iH(t-t_0)/\hbar] \times \exp(-iH_\alpha t_0/\hbar) . \tag{2.29}$$

The S-matrix operator is defined as

$$\hat{S}_{\beta\alpha} \equiv \lim_{t\geq t_f; t'\leq t_0} \hat{U}^{\beta\alpha}_I(t,t') . \tag{2.30}$$

Due to energy conservation, there are no transitions between different energy states, i.e.,

$$\lim_{t\geq t_f} \langle \phi^J_{\beta nj\Omega}(E)|\hat{U}^{\beta\alpha}_I(t,t_0)|\phi^J_{\alpha n_0j_0m_0}(E_0)\rangle = 0 \quad \text{unless } E = E_0 . \tag{2.31}$$

We therefore define the on-shell S-matrix as

$$S^J_{\beta\alpha}(nj\Omega|n_0j_0m_0|E)\delta(E-E_0) = \lim_{t\geq t_f} \langle \phi^J_{\beta nj\Omega}(E)|\hat{U}^{\beta\alpha}_I(t,t_0)|\phi^J_{\alpha_{n_0}j_0m_0}(E_0)\rangle . \tag{2.32}$$

We then substitute Eq. (2.32) into Eq. (2.28) and integrate over E_0 to get

$$\tilde{I}^J_{\beta\alpha}(nj\Omega|n_0j_0m_0|E) = \mathcal{A}(E)\exp[-iE(t-t_0)/\hbar]S^J_{\beta\alpha}(nj\Omega|n_0j_0m_0|E) , \quad t\geq t_f \tag{2.33}$$

or

$$S^J_{\beta\alpha}(nj\Omega|n_0j_0m_0|E) = \frac{1}{\mathcal{A}(E)}\tilde{I}^J_{\beta\alpha}(nj\Omega|n_0j_0m_0|E) \times \exp[iE(t-t_0)/\hbar], \quad t\geq t_f . \tag{2.34}$$

In order to convert this expression to one that makes use of our coordinate representation wave packet, we insert the identity in the form

$$1 = \sum_{j'\Omega'} \int_0^\infty dR_\beta \int_0^\infty dr_\beta |(j'\Omega'Rr)_\beta\rangle\langle(j'\Omega'Rr)_\beta| \tag{2.35}$$

into Eq. (2.25a), which yields

$$\tilde{I}^J_{\beta\alpha}(nj\Omega|n_0j_0m_0|E) = \lim_{t\geq t_f} \sum_{j'\Omega'} \int_0^\infty dR_\beta \int_0^\infty dr_\beta \langle \phi^J_{\beta nj\Omega}(E)|(j'\Omega'Rr)_\beta\rangle\langle(j'\Omega'Rr)_\beta|\psi^J_{n_0j_0m_0}(t)\rangle . \tag{2.36}$$

This can be modified by using the relations given in Eqs. (2.22) and (2.26) to give

$$\tilde{I}^J_{\beta\alpha}(nj\Omega|n_0j_0m_0|E) = \lim_{t\geq t_f} \left[\frac{\mu_\beta}{\hbar^2k}\right]^{1/2} \sum_{\Omega'} \int_0^\infty dR_\beta \int_0^\infty dr_\beta [\mathcal{J}^{Jj}_{\Omega\Omega'}(kR_\beta)]^* \varphi^\beta_{nj}(r_\beta)\chi^J_\beta(j\Omega'|n_0j_0m_0|R_\beta,r_\beta,t) \tag{2.37}$$

$$= \left[\frac{\mu_\beta}{\hbar^2k}\right]^{1/2} I^J_{\beta\alpha}(nj\Omega|n_0j_0m_0|k) . \tag{2.38}$$

If we compare Eqs. (2.9) and (2.27) and recall that

$$E=\frac{\hbar^2 k_0^2}{2\mu_\alpha}+\epsilon^\alpha_{n_0 j_0}=\frac{\hbar^2 k^2}{2\mu_\beta}+\epsilon^\beta_{nj} ,$$

we can make the identification

$$\mathcal{A}(E)=\left[\frac{\mu_\alpha}{\hbar^2 k_0}\right]^{1/2} A(k_0) . \tag{2.39}$$

This leads to the final working expression for the S-matrix elements,

$$S^J_{\beta\alpha}(nj\Omega|n_0 j_0 m_0|k)=\left[\frac{k_0\mu_\beta}{k\mu_\alpha}\right]^{1/2}\frac{1}{A(k_0)} \times\exp\left[i\left[\frac{\hbar^2 k_0^2}{2\mu_\alpha}+\epsilon^\alpha_{n_0 j_0}\right](t-t_0)/\hbar\right] \times I^J_{\beta\alpha}(nj\Omega|n_0 j_0 m_0|k) , \tag{2.40}$$

where $I^J_{\beta\alpha}(nj\Omega|n_0 j_0 m_0|k)$ was defined in Eq. (2.38).

Using the $S^J_{\beta\alpha}(nj\Omega|n_0 j_0 m_0|k)$, we can write expressions for the differential scattering amplitudes and cross sections. The differential scattering amplitude is given by

$$f_{\beta\alpha}(nj\Omega k|n_0 j_0 m_0|\hat{R}_\beta) =\frac{i}{2\sqrt{kk_0}}\sum_J (2j+1)D^J_{\Omega m_0}(\hat{R}_\beta)T^J_{\beta\alpha}(nj\Omega|n_0 j_0 m_0|k) , \tag{2.41}$$

where the T-matrix elements are defined by the equation

$$T^J_{\beta\alpha}(nj\Omega|n_0 j_0 m_0|k)=\delta_{nn_0}\delta_{jj_0}\delta_{\Omega m_0} -S^J_{\beta\alpha}(nj\Omega|n_0 j_0 m_0|k) . \tag{2.42}$$

The state-to-state differential cross section is given by

$$\frac{d\sigma_{\beta\alpha}}{d(\hat{R}_\beta)}(nj\Omega k\leftarrow n_0 j_0 m_0)=\frac{k}{k_0}|f_{\beta\alpha}(nj\Omega k|n_0 j_0 m_0|\hat{R}_\beta)|^2 . \tag{2.43}$$

A potential problem that arises when resonances are present is that part of the wave packet may have propagated quite far down the asymptotic channel before the parts caught in the resonance finally leave the interaction region. Methods that avoid having to use large grids in this situation have been developed by Metiu and coworkers[21] and Neuhauser and Baer.[30] We take advantage of the linear nature of the Schrödinger equation in the following way: We propagate the wave function $\psi(R,t)$ to a time t_i when it has started to leave the interaction region. The wave function is broken up into two pieces as follows:

$$\psi(R,t_i)=f(R)\psi(R,t_i)+[1-f(R)]\psi(R,t_i) , \tag{2.44}$$

where $f(R)$ is a function that takes the value zero in the interaction region, the value one in the far asymptotic region, and smoothly goes from zero to one in some intermediate region. (We define the dividing line between the interaction and asymptotic regions as R_V, where the interaction potential is practically zero for $R>R_V$.) The portion of the wave function $f(R)\psi(R,t_i)$ has completely left the interaction region so we can calculate and save its contribution to the S matrix [using Eq. (2.40)] and then discard $f(R)\psi(R,t_i)$. The remaining portion of the wave function, $[1-f(R)]\psi(R,t_i)$, is next propagated for another time step and broken up again using f and $(1-f)$. The asymptotic region component is analyzed and its contribution to the S matrix is added to the previously calculated piece. This process is repeated until all of the wave function has been analyzed.

The function $f(R)$ has to satisfy two requirements. First, it must be smooth enough so that it does not introduce spurious high-frequency components into the S matrix when we analyze $f(R)\psi(R,t)$. Second, the transition region must be relatively narrow so that we do not have to use long grids to capture a significant region where $f(R)=1$. The following function works well in practice.[29,30] We make the definition

$$y(R)=\frac{R-\bar{R}}{W_R} , \tag{2.45}$$

where the transition from zero to one starts at $\bar{R}$ and W_R is the width of the transition region. The value of $\bar{R}$ must be greater than R_V and W_R should typically be 1–2 Å. The function f is then defined as[30]

$$f(R)=\begin{cases}0, & y(R)<0\\ 10y^3-15y^4+6y^5, & 0<y(R)<1\\ 1, & y(R)>1 .\end{cases} \tag{2.46}$$

E. Transformation between arrangements

In this section we show how to calculate the channel wave packets

$$\chi^J_\beta(j',\Omega'|n_0 j_0 m_0|R',r',t)$$

in arrangement β, given the corresponding functions

$$\chi^J_\alpha(j,\Omega|n_0 j_0 m_0|R,r,t)$$

in arrangement α. In practice, α always designates the initial arrangement. To simplify notation, we will drop the dependence on the initial state $(n_0 j_0 m_0)$ in the following derivation. Additionally, coordinates in the β arrangement are primed and those in the α arrangement are unprimed. The formulas derived here are valid for either the symmetrized or the unsymmetrized channel wave packets. In the following equations, Ω ranges over both positive and negative values. The details of rotating coordinates from one set of axes to another were considered by many people.[43] A very clear discussion of the relevant coordinate transformations has been given by Miller.[44] However, in that context, it leads to coupled integro-differential equations that are not easily propagated by standard time-independent close coupling (CC) methods. In the present approach, we simply wish to use the wave packet at time t as the initial condition to con-

tinue propagating using the Jacobi coordinates of the product arrangement. Thus, one simply interpolates from one grid to another, and no nonlocal matrix elements are produced.

We first make the following definitions: The full coordinate representation wave packets in arrangement α are given by

$$\psi_\alpha^{J\Omega}(R,r,\gamma,t)=\sum_j Y_{j\Omega}(\gamma,0)\chi_\alpha^J(j,\Omega|R,r,t) , \quad (2.47a)$$

where the $\chi_\alpha^J(j,\Omega|R,r,t)$ and $\psi_\alpha^{J\Omega}(R,r,\gamma,t)$ are quantized along the α arrangement body-frame axis. The full center-of-mass-frame wave function in arrangement α is given by

$$\Psi_\alpha^{Jm_0}(R,r,\gamma|\xi,\theta,\zeta|t)=\frac{1}{rR}\sum_\Omega \psi_\alpha^{J\Omega}(R,r,\gamma,t)[D^J_{\Omega m_0}(\xi,\theta,\zeta)]^* , \quad (2.47b)$$

where the $\Psi_\alpha^{Jm_0}(R,r,\gamma|\xi,\theta,\zeta|t)$ are quantized along the space-fixed axis and are expressed in terms of the α arrangement coordinates. The full coordinate representation wave packets in arrangement β are given by

$$\psi_\beta^{J\Omega'}(R',r',\gamma',t)=r'R'\frac{2J+1}{8\pi^2}\int_0^{2\pi}d\xi'\int_{-1}^{1}d(\cos\theta')\int_0^{2\pi}d\zeta' D^J_{\Omega' m_0}(\xi',\theta',\zeta')\Psi_\beta^{Jm_0}(R',r',\gamma'|\xi',\theta',\zeta'|t) , \quad (2.47c)$$

where the $\Psi_\beta^{Jm_0}(R',r',\gamma'|\xi',\theta',\zeta'|t)$ are also quantized along the space-fixed axis but are expressed in terms of the β arrangement coordinates. The factors (rR) and $(r'R')$ are a consequence of the same term in Eq. (2.1). The rotational close-coupled channel wave packets in arrangement β are given by

$$\chi_\beta^J(j',\Omega'|R',r',t)=2\pi\int_{-1}^{+1}d(\cos\gamma')Y_{j'\Omega'}(\gamma',0)\psi_\beta^{J\Omega'}(R',r',\gamma',t) , \quad (2.47d)$$

where the $\psi_\beta^{J\Omega'}(R',r',\gamma',t)$ and $\chi_\beta^J(j',\Omega'|R',r',t)$ are quantized along the β arrangement body-frame axis. Notice that Eq. (2.47d) is the inverse of (2.47a) and that (2.47c) is the inverse of (2.47b) except for the arrangement number. The important point to note is that the functions $\Psi_\alpha^{Jm_0}(R,r,\gamma|\xi,\theta,\zeta|t)$ and $\Psi_\beta^{Jm_0}(R',r',\gamma'|\xi',\theta',\zeta'|t)$ are *identical* when $(R,r,\gamma,\xi,\theta,\zeta)$ and $(R',r',\gamma',\xi',\theta',\zeta')$ describe the same point in space. Therefore, Eqs. (2.47) constitute a scheme for calculating $\chi_\beta^J(j',\Omega'|R',r',t)$, given $\chi_\alpha^J(j,\Omega|R,r,t)$. However, it is never necessary to explicitly calculate the function Ψ^{Jm_0}, as we now show. Equation (2.47b) can be rewritten as

$$\begin{aligned}\Psi_\beta^{Jm_0}(R',r',\gamma'|\xi',\theta',\zeta'|t)&=\sum_\Omega\frac{1}{rR}\psi_\alpha^{J\Omega}(R,r,\gamma,t)[D^J_{\Omega m_0}(\xi,\theta,\zeta)]^*|_{(R,r,\gamma,\xi,\theta,\zeta)=(R',r',\gamma',\xi',\theta',\zeta')}\\&=\sum_\Omega\frac{1}{rR}\psi_\alpha^{J\Omega}(R,r,\gamma,t)|_{(R,r,\gamma)=(R',r',\gamma')}\sum_{\Omega''}[D^J_{\Omega'' m_0}(\xi',\theta',\zeta')]^*[D^J_{\Omega''}(\tilde\xi,\tilde\theta,\tilde\zeta)]^* , \end{aligned}\quad (2.48)$$

where in the second step, we have made use of the closure property of the Wigner rotation matrices.[40] The notation

$$(R,r,\gamma,\xi,\theta,\zeta)=(R',r',\gamma',\xi',\theta',\zeta')$$

means that the functions of the unprimed coordinates will be evaluated at the point in space specified by the primed coordinates. Here, $(\tilde\xi,\tilde\theta,\tilde\zeta)$ transforms (ξ',θ',ζ') into (ξ,θ,ζ). One can show that $(\tilde\xi,\tilde\theta,\tilde\zeta)=(0,\tilde\theta,0)$ and that $\tilde\theta$ only depends on the internal coordinates and therefore is independent of the (ξ',θ',ζ') that rotate the plane of the atoms with respect to the space-fixed coordinate axes. Refer to Fig. 1. Now, if we combine Eq. (2.48) with (2.47c) and use the orthogonality property of the Wigner rotation matrices,[40] we arrive at the following identity:

$$\psi_\beta^{J\Omega'}(R',r',\gamma',t)=\frac{r'R'}{rR}\sum_\Omega\psi_\alpha^{J\Omega}(R,r,\gamma,t)|_{(R,r,\gamma)=(R',r',\gamma')}\times d^J_{\Omega\Omega'}(\tilde\theta) . \quad (2.49)$$

We next substitute Eq. (2.47a) into (2.49) to yield

$$\psi_\beta^{J\Omega'}(R',r',\gamma',t)=\frac{r'R'}{rR}\sum_{j\Omega}Y_{j\Omega}(\gamma,0)\chi_\alpha^J(j,\Omega|R,r,t)|_{(R,r,\gamma)=(R',r',\gamma')}\times d^J_{\Omega\Omega'}(\tilde\theta) . \quad (2.50)$$

Equations (2.50) and (2.47d) provide a scheme for transforming from the α to the β representation of the channel wave packets.

Next, we need an accurate, efficient algorithm for evaluating the functions $\chi_\alpha^J(j,\Omega|R,r,t)$ at points corresponding to (R',r',γ'). The channel packets are known only on a grid of points (R_ν,r_λ) that do not line up with the corresponding grid of points in the reactive arrangements, forcing us to interpolate. Because we will subsequently propagate the β arrangement channel packets, they must be calculated accurately in both configuration and momentum space. We use Fourier-transform interpolation because it best satisfies these dual accuracy requirements. (A possible alternative is the interpolation method of Bisseling and Kosloff.[45]) We could do the in-

terpolation in both R and r simultaneously, but this proves to be expensive numerically. We instead factor the evaluation of Eq. (2.50) into several steps, which produces an algorithm that scales linearly with problem size.

We first fast Fourier transform $\chi_\alpha^J(j,\Omega|R,r,t)$ in the R coordinate only to produce the functions

$$\hat{\chi}_\alpha^J(j,\Omega|K_n,r_p,t)=\sum_s \exp(iK_nR_s)\chi_\alpha^J(j,\Omega|R_s,r_p,t) \ . \tag{2.51}$$

We next transform to a new set of functions given by

$$\Phi_\alpha^{J\Omega}(r_p,r_{p'}',\rho_m) = \frac{r_{p'}'}{\tilde{R}}\frac{1}{N_R}\sum_j Y_{j\Omega}(\tilde{\gamma},0) \times \sum_n \exp(-iK_n\tilde{R})\hat{\chi}_\alpha^J(j,\Omega|K_n,r_p,t) \ , \tag{2.52}$$

where ρ is the angle between $\hat{r}$ and $\hat{r}'$. The $\Phi_\alpha^{J\Omega}$ functions are calculated on a grid of points $(r_p,r_{p'}',\rho_m)$ corresponding to the r grid points in arrangement α, and the r' grid points in arrangement β. The ρ points are chosen appropriately for performing Gauss-Legendre quadrature. The variables $\tilde{R}$ and $\tilde{\gamma}$ are the values of R and γ that correspond to the point $(r_p,r_{p'}',\rho_m)$. The factor $r_{p'}'/\tilde{R}$ is the transformation Jacobian between the coordinates (R,r,γ) and (r,r',ρ). The Φ functions are now expanded in Legendre polynomials as follows:

$$\Phi_\alpha^{J\Omega}(L|r_p,r_{p'}')=\frac{2L+1}{2}\int_{-1}^{+1}d(\cos\rho)P_L(\cos\rho) \times\Phi_\alpha^{J\Omega}(r_p,r_{p'}',\rho) \tag{2.53}$$

and then Fourier transformed from r to k as follows:

$$\hat{\Phi}_\alpha^{J\Omega}(L|k_l,r_{p'}')=\sum_p \exp(ik_lr_p)\Phi_\alpha^{J\Omega}(L|r_p,r_{p'}') \ . \tag{2.54}$$

The final step in the transformation that produces the desired function $\psi_\beta^{J\Omega'}(R_{s'}',r_{p'}',\gamma_{q'}',t)$ is

$$\psi_\beta^{J\Omega'}(R_{s'}',r_{p'}',\gamma_{q'}',t)=\frac{r_{p'}'R_{s'}'}{\tilde{r}\tilde{R}}\frac{R_{s'}'}{\tilde{r}}\sum_\Omega d_{\Omega\Omega'}^J(\tilde{\theta})\sum_L P_L(\cos\tilde{\rho}) \times\frac{1}{N_r}\sum_l \exp(-ik_l\tilde{r})\hat{\Phi}_\alpha^{J\Omega}(L|k_l,r_{p'}') \ , \tag{2.55}$$

where $\tilde{r}$, $\tilde{R}$, and $\tilde{\rho}$ are the values of r, R, and ρ corresponding to the point $(R_{s'}',r_{p'}',\gamma_{q'}')$. As before, the $\gamma_{q'}'$ points are chosen to be appropriate for performing Gauss-Legendre quadrature. [Note that in Eqs. (2.55) and (2.52) because the target R or r points are not uniformly spaced, a fast Fourier transform cannot be used.] We can now substitute ψ_β into Eq. (2.47d) to calculate the β arrangement channel packets on the appropriate numerical grid.

Notice that there is no requirement that the range of the grids, the number of grid points, or the number of (j,Ω) states be the same in arrangements α and β. In fact, these quantities will in general differ from one arrangement to another, being adjusted to best treat the atom-diatom pair corresponding to that arrangement.

F. Absorbing potentials

As mentioned above, reactive portions of the wave packet will eventually move off the numerical grid used to describe the nonreactive asymptotic arrangement (and vice versa). If no special precautions are taken, the portions of the wave packet that reach the edge of the grid will be unphysically reflected back onto the inelastic grid, invalidating the results of the calculation. This problem is easily solved by employing an imaginary, optical potential that will absorb any part of the wave packet that approaches the grid boundary. In the present work, we use the method of Neuhauser and Baer that is described more fully in Ref. 28. We simply add an extra diagonal term to the channel Hamiltonian

$$H^J(j'\Omega'|j\Omega)\rightarrow H^J(j'\Omega'|j\Omega)+V_{\rm opt}(r)\delta_{jj'}\delta_{\Omega\Omega'} \ , \tag{2.56}$$

where

$$V_{\rm opt}(r)=\begin{cases} -i\bar{V}_{\rm opt}\left[1-\dfrac{r_{\rm max}-r}{\Delta r}\right], & r_{\rm max}-\Delta r\le r\le r_{\rm max} \\ 0, \quad \text{otherwise} \ , \end{cases} \tag{2.57}$$

and where $\bar{V}_{\rm opt}$ gives the strength of the absorbing potential in units of energy and Δr gives its range. This simple linear form is found to work quite well for relatively small values of $\bar{V}_{\rm opt}$ and Δr. Values for these parameters can be estimated from the inequality[28]

$$E_{\rm tr}^{1/2}/(\Delta r\sqrt{8\mu})<\bar{V}_{\rm opt}<(\Delta r\sqrt{8\mu})E_{\rm tr}^{3/2} \ , \tag{2.58}$$

where $E_{\rm tr}$ is the translational energy in the r direction. Note that Eq. (2.58) can only be used as an estimate because the wave packets we are using contain a wide range of energies. Typical values for the calculations reported here are $\bar{V}_{\rm opt}=1$ eV and $\Delta r=1$ Å.

III. COMPUTATIONAL SCHEME

In Sec. II we described the tools needed to form, propagate, and analyze wave packets in the three different inelastic arrangements. By inelastic, we specifically mean that the wave packet is described by the variables R, r, and γ, where R may extend to large values but where the range of r is restricted. Hence, a large number of grid points is needed in one dimension only. In contrast, in order to simultaneously describe the full reactive problem, large numbers of grid points are needed in at least two dimensions, greatly increasing the sizes of the arrays needed to describe the potential and the wave packets. In this section we describe how to combine the tools developed in Sec. II for inelastic scattering into an algorithm for performing reactive scattering calculations.

The first step is to calculate the initial ($t=0$) parity-conserving channel wave packets for the initial arrangement, using the equations given in Secs. II B and II C.

These are calculated on a uniform rectangular grid in R and r, where R extends from $R_{\min}$ to $R_{\max}$ and r extends from $r_{\min}$ to $r_{\max}$. $R_{\min}$ is set to zero. Although most of the wave function is excluded from the small R region due to the highly repulsive potential, the collinear symmetric stretch configuration will be sampled by the $l=0$ component of the wave packet. The value of $r_{\min}$ is chosen small enough so that the wave function will never sample smaller values due to the highly repulsive potential. $R_{\max}$ is chosen to be far enough beyond the point where $f(R)$ reaches the value one (see Sec. II D) to fit a significant portion of the wave function. We will describe shortly how the value of $r_{\max}$ is chosen. Once the initial channel wave packets are calculated, they are propagated into the interaction region using the methods described in Sec. II A. Typically, the propagation is broken up into between 20 and 40 time steps.

The next step is the crucial one for incorporating reaction. We define the "grid overlap region" as that volume of (R,r,γ) space that is simultaneously included in the inelastic grids for each of the three arrangements. The overlap region will include the strong interaction region plus some portion of the near asymptotic channel for each arrangement. (Notice that the wave packets and the Hamiltonian are expressed in terms of the quantum numbers j and Ω rather than the angle γ, but this is unimportant for the present discussion. The range of γ in each arrangement is $0\leq\gamma<\pi$.) We choose the grids (and hence the overlap region) to be large enough so that over some interval in time, the entire wave function will fit in the overlap region. Once the channel wave packets (numerically stored on the grid corresponding to the initial arrangement) are completely contained in the overlap region, they are written to disk and saved. The nonreactive S-matrix elements are calculated by performing the outgoing propagation on the initial arrangement grid and carrying out the final-state analysis described in Sec. II D. The optical potential absorbs all parts of the wave packet that move into the reactive arrangement channels. In the next stage of the calculation, the previously stored wave function (which lies completely in the overlap region) is read back from disk and transformed so that it is expressed in terms of the coordinates for one of the reactive arrangements, using the method of Sec. II E. The outgoing propagation in that arrangement is then performed, using the Hamiltonian appropriate to that arrangement, and the reactive S-matrix elements are calculated. If the two reactive arrangements are not identical, this procedure is repeated for the other arrangement.

There are several comments we need to make about fitting the wave packets into the grid overlap region prior to the transformation step. The fact that the wave function must lie completely within the overlap region sets a lower bound on the value of $r_{\max}$. This bound, of course, depends on the size of the wave packet when it enters the interaction region, which in turn depends on factors such as the initial width of the wave packet and the nature of the potential. An additional requirement is that no part of the wave packet should lie in a region where the optical potential for any arrangement is nonzero. This forces a further increase in the value of $r_{\max}$. Finally, to make the algorithm somewhat more robust, the "good" overlap region (total region minus that where the optical potentials are nonzero) should be large enough to contain fully the wave function for two or three time steps. This necessitates a further increase in $r_{\max}$. Once the grid size has been fixed, however, deciding when to perform the coordinate transformation is relatively simple. At each time step, we calculate the fraction of the wave function in the good overlap region and when this value exceeds some predetermined limit (typically 0.999), the wave function is saved.

It is tempting to use extremely narrow wave packets to reduce the volume that must be included in the overlap region, but there are both theoretical and practical restrictions on how far it is possible to go in this direction. The major theoretical problem is that a narrow spatial wave packet will be broad in momentum space and therefore will spread very rapidly, negating its intended utility. In addition, this packet will contain large-momentum components, requiring that the maximum value of the momentum to be sampled be large. This value is $\pi/\Delta R$, where ΔR is the grid spacing. Hence, small spacings in the configuration space grid would be required. Another way of saying this is that the wave packet must spread over enough grid points so that its numerical representation is smooth. Otherwise, numerical instabilities will occur. A very narrow wave packet would then require a correspondingly fine grid spacing.

This method for incorporating reaction is exact in principle. However, errors can be introduced in the following way: Parts of the wave packet that will eventually end up in arrangement β can in principle pass through the interaction region, travel some distance in the direction of the β' arrangement, turn around and re-enter the interaction region, and finally exit permanently into the β arrangement. If the inelastic grid for the β arrangement does not extend sufficiently far in the β' direction to capture the momentary excursion of the wave packet in that direction, then part of the contribution to the β arrangement S matrix will be lost. Notice that this fact implies a lower bound on the value of $r_{\max}$ that may be different from that described above. For the test calculation we describe in Sec. IV, we found that the lower bound forced on us by the requirement that the entire wave packet fit in the overlap region was much more stringent than that required to capture these "indirect" pieces of the wave packet. (Note that the size of our overlap region is related to the idea of a "point of no return" in transition-state theory.[46] There exists a minimal surface in configuration space surrounding the interaction region that has the property that any part of the wave function that crosses it will never return to the interaction region.)

We can compare the effort required to perform the complete inelastic-plus-reactive calculation with that needed to perform a completely inelastic calculation. In the latter, we must perform one incoming propagation and one outgoing, that are of roughly identical cost, which we designate P_{in}. The final-state analysis must be performed once, at a cost of F_{in}. For an atom-homonuclear diatom reactive calculation, we must perform the incoming propagation ($\mathcal{N}_{\text{cost}}=P_r$), the outgoing

nonreactive propagation ($\mathcal{N}_{\rm cost}=P_r$), the outgoing reactive propagation ($\mathcal{N}_{\rm cost}=2P_r$), an interpolation ($\mathcal{N}_{\rm cost}=I_{\alpha\beta}$) and the final-state analysis in the nonreactive arrangement ($\mathcal{N}_{\rm cost}=F_r$), and the reactive arrangement ($\mathcal{N}_{\rm cost}=2F_r$). The factors of 2 in the reactive channel are due to the fact that a homonuclear diatom in the nonreactive arrangement can only be in either even or odd j states, but in the reactive arrangement, both even and odd states will be populated. To summarize, the cost of the inelastic calculation is approximately

$$\mathcal{N}_{\rm cost}(\mathcal{I})\sim 2P_{\rm in}+F_{\rm in}$$

and the cost of the reactive calculation is approximately

$$\mathcal{N}_{\rm cost}(\mathcal{R})\sim 4P_r+2F_r+I_{\alpha\beta}\ .$$

The half-propagation in the reactive case (P_r) will be on the order of twice that of the inelastic calculation because the grid in r must extend on the order of twice as far to insure that the wave packet can be enclosed in the overlap region. Except for small calculations, the propagation step dominates, so that the total reactive calculation will be on the order of four times more expensive than the purely inelastic calculation (for the identical system). One can easily show that this factor of 4 also holds true for the case where all three atoms are dissimilar.

IV. NUMERICAL TEST

In this section we present the results of a sample calculation using the method described in the previous sections. The system we examine is $H+H_2$ ($J=0$) on the Liu-Siegbahn-Truhlar-Horowitz (LSTH) potential-energy surface.[47] The state-to-state transition probabilities for this system are well known,[2(b)] so these calculations provide a good check on the accuracy of our method.

A number of parameters are used in the calculation and we will discuss the most important ones here. The values used are summarized in Table I. They have not been optimized for speed of execution, and the basis set and grids in particular are probably considerably larger than they need to be. To begin, the grids are determined by the number of grid points, N_R in the R direction and N_r in the r direction. We use $N_R=256$ and $N_r=64$. The R grid extends from 0 to 20 Å, and the r grid from 0.15 to 4.5 Å. The maximum value of j used in the expansion of the wave function (designated $j_{\rm max}$) was set equal to 22, which allows for several closed channels at the highest energies in the wave packet. The width of the initial wave packet, σ, was set equal to 0.55 Å. This was sufficiently narrow so that the entire wave function fit into the overlap region between the inelastic and reactive grids over a reasonably long period of time. The center energy of the wave packet, E_0, was set to 1.0 eV for the high-energy run and 0.75 eV for the low-energy run and the initial vibration-rotation state was $n_0=j_0=0$. The corresponding momentum wave packet was quite broad so that from a single run ($E_0=1.0$ eV), we were able to get accurate probabilities over the entire energy range, 0.8 eV $<E<$ 1.3 eV. The packet was initially centered at $R_0=8.9$ Å. The time step used was approximately 0.5×10^{-14} s and the total propagation time was 25×10^{-14} s. The wave packet was stopped at 5.0×10^{-14} s for the interpolation, at which time the fraction of the wave packet in the overlap region was equal to 0.999 93.

After the interpolation, the norm of the wave packet on the reactive grid was 0.999 92, indicating that the interpolation error is small. The final-state analysis was started at 10×10^{-14} s. As would be expected, the components of the S matrix for high kinetic energy (high E, low n,j) converged faster in time because they reached the asymptotic region sooner.

In Table II we give the probabilities summed over j for several energies and compare them with the previously reported values.[2(b)] The comparison is good at most energies. In Table III we give our results as a function of n and j for several energies. Except for numbers that have very small size, our values agree with the previous ones to about 8% in most cases, which is within the previous error estimate. In Fig. 2 we show the inelastic, and in Fig. 3, the reactive results (summed over j) as a function of energy and compare them with the results of Ref. 2(b). We should emphasize that the entire curve, made up of better than 250 individual energies from 0.5 to 1.3 eV,

TABLE I. Typical physical and numerical run parameters.

Variable	Value	Description
J	0	Total angular momentum
$j_{\rm max}$	22	Maximum value of j used
j_0	0	Initial rotor quantum number
n_0	0	Initial vibrational quantum number
m_0	0	Initial projection quantum number
N_R	256	Number of points in the R grid
$R_{\rm min}$	0.0 Å	Minimum value of the R grid
$R_{\rm max}$	20.0 Å	Maximum value of the R grid
N_r	64	Number of points in the r grid
$r_{\rm min}$	0.15 Å	Minimum value of the r grid
$r_{\rm max}$	4.80 Å	Maximum value of the r grid
σ	0.55 Å	Width of the initial wave packet
E_0	1.0 eV	Initial mean energy of the wave packet
R_0	8.9 Å	Location of center of wave packet at $t=0$

TABLE II. $H+H_2$ transition probabilities ($P_{00\to0}$,$P_{00\to1}$) for several energies at selected energies compared with previously published results. Values after the semicolon denote $P_{00\to1}$.

Energy (eV)	Inelastic [Ref. 2(b)]	This work	Reactive [Ref. 2(b)]	This work
0.50		0.999	2(−4)	1(−4)
0.55		0.997	0.003	0.003
0.575		0.988	0.011	0.012
0.60		0.962	0.036	0.038
0.625		0.902	0.10	0.098
0.65		0.794	0.20	0.206
0.70		0.653	0.34	0.342
0.80	0.633;4(−4)[a]	0.634;1(−7)	0.36;6(−6)	0.359;3(−6)
0.85		0.589;2(−5)	0.41;3(−6)	0.405;7(−5)
0.90	0.521;4(−4)	0.524;5(−4)	0.47;3(−4)	0.479;3(−4)
0.95		0.512;0.010	0.47;0.011	0.469;0.010
0.96		0.513;0.020	0.44;0.023	0.449;0.022
0.98		0.510;0.047	0.37;0.066	0.377;0.072
1.00	0.485;0.046	0.482;0.044	0.39;0.077	0.394;0.078
1.05		0.459;0.017	0.44;0.061	0.466;0.052
1.10	0.423;0.019	0.430;0.018	0.50;0.051	0.491;0.060
1.20	0.395;0.048	0.395;0.044	0.45;0.10	0.441;0.109
1.30		0.338;0.035	0.50;0.10	0.492;0.110

[a] 4(−4) denotes 4×10^{-4}.

TABLE III. Transition probabilities at selected energies. Numbers in parentheses are as follows: (arrangement number, vibrational state, rotational state). The initial state was (1,0,0), $J=0$.

Final state[a]	$E_{tot}=0.80$	$E_{tot}=0.90$	$E_{tot}=1.00$	$E_{tot}=1.10$	$E_{tot}=1.20$
(1,0,0)	3.51(−1)[b]	2.38(−1)	2.34(−1)	1.92(−1)	1.94(−1)
(1,0,2)	1.78(−1)	1.31(−1)	1.27(−1)	8.58(−2)	6.56(−2)
(1,0,4)	1.04(−1)	1.32 (−1)	7.61(−2)	8.43(−2)	7.99(−2)
(1,0,6)	2.45(−3)	2.26(−2)	4.48(−2)	6.07(−2)	4.25(−2)
(1,0,8)	4.10(−6)	2.45(−5)	6.23(−4)	6.55(−3)	1.32(−2)
(1,0,10)				6.03(−8)	4.28(−5)
(1,1,0)	1.34(−5)	2.93(−4)	2.31(−2)	3.86(−3)	7.34(−3)
(1,1,2)		2.04(−4)	2.10(−2)	1.11(−2)	1.37(−2)
(1,1,4)			1.95(−4)	3.36(−3)	2.21(−2)
(1,1,6)				6.79(−7)	6.45(−4)
(2,0,0)	2.38(−2)	4.10(−2)	4.20(−2)	5.60(−2)	5.59(−2)
(2,0,1)	5.43(−2)	7.89(−2)	7.33(−2)	9.41(−2)	8.31(−2)
(2,0,2)	5.31(−2)	5.44(−2)	3.73(−2)	3.62(−2)	2.19(−2)
(2,0,3)	3.29(−2)	2.97(−2)	8.74(−3)	7.17(−3)	4.26(−3)
(2,0,4)	1.25(−2)	2.11(−2)	1.10(−2)	1.52(−2)	2.31(−2)
(2,0,5)	2.58(−3)	1.14(−2)	1.59(−2)	1.69(−2)	1.82(−2)
(2,0,6)	2.46(−4)	2.89(−3)	7.52(−3)	1.27(−2)	6.74(−3)
(2,0,7)	6.71(−6)	2.46(−4)	1.66(−3)	5.93(−3)	4.60(−3)
(2,0,8)	2.73(−9)	3.52(−6)	1.00(−4)	1.12(−3)	2.37(−3)
(2,0,9)		9.33(−10)	7.21(−7)	4.46(−5)	4.06(−4)
(2,0,10)				1.37(−7)	1.01(−5)
(2,1,0)	1.40(−8)	3.57(−5)	1.08(−2)	5.97(−3)	1.23(−2)
(2,1,1)		6.73(−5)	1.72(−2)	9.44(−3)	1.57(−2)
(2,1,2)		2.67(−5)	9.16(−3)	9.54(−3)	5.49(−3)
(2,1,3)		8.57(−7)	1.67(−3)	4.05(−3)	8.52(−3)
(2,1,4)			5.86(−5)	1.12(−3)	9.10(−3)
(2,1,5)			1.75(−8)	6.88(−5)	3.12(−3)
(2,1,6)				1.74(−8)	2.04(−4)
(2,1,7)					2.56(−7)

[a] All energies are in eV.

[b] 3.51(−1) denotes 3.51×10^{-1}.

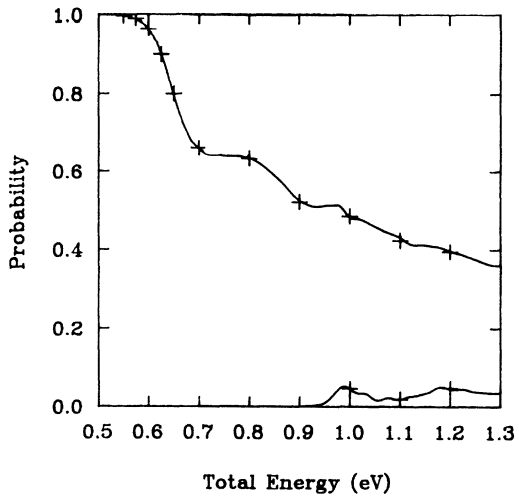

FIG. 2. Inelastic scattering probabilities $P_{in}(v_0,j_0 \rightarrow v|E)$ for the $H+H_2$ system ($J=0$), summed over rotational quantum number j, as a function of total energy in eV. The LSTH (Ref. 43) potential surface was used. The initial state was $j_0=0$, $v_0=0$. The upper curve gives the results for $v=0$ and the lower curve for $v=1$. The plus signs give the previously calculated converged results from Ref. 2(b).

was calculated in only two runs. The agreement in the vicinity of the 0.98-eV resonance is especially good. In Fig. 4 we show the n,j resolved inelastic probabilities as a function of energy for several representative states and compare them with the previous reported values. The curves are very oscillatory, but all of this structure appears to be real, as evidenced by the good agreement with the known values. The corresponding reactive results are shown in Fig. 5. An interesting point about this figure is that only the states $j=0$, 1, and 2 participate in the resonance at 0.98 eV. No special features occur at that energy for $j \geq 3$.

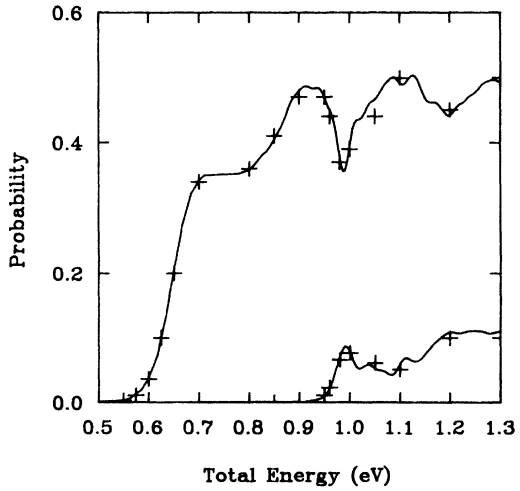

FIG. 3. Reactive scattering probabilities $P_r(v_0,j_0 \rightarrow v|E)$ corresponding to the inelastic results in Fig. 2. Note the good agreement with the previous results in the vicinity of the 0.987-eV resonance.

In order to accurately capture the resonance in this calculation, it was necessary to insure that the wave packet was propagated for a sufficiently long time. In Fig. 6 we show the reactive probability ($n=0$, summed over j) at the resonance minimum (0.987 eV) as a function of time step after the final analysis started. The resonance gets progressively deeper as time goes on, but finally levels off. Further propagation would deepen the resonance a slight bit more; however, the value had converged to well below our level of numerical error. In Fig. 7 we show the probability as a function of energy at three times (step 11, dotted curve; step 21, dashed curve; step 31, solid curve). From these curves, one can see that the resonance steepens at the same time that it deepens, just as one would expect.

As we have stated, the parameters used in these calculations and the code itself have not been optimized for speed. However, it is useful to look at the computational

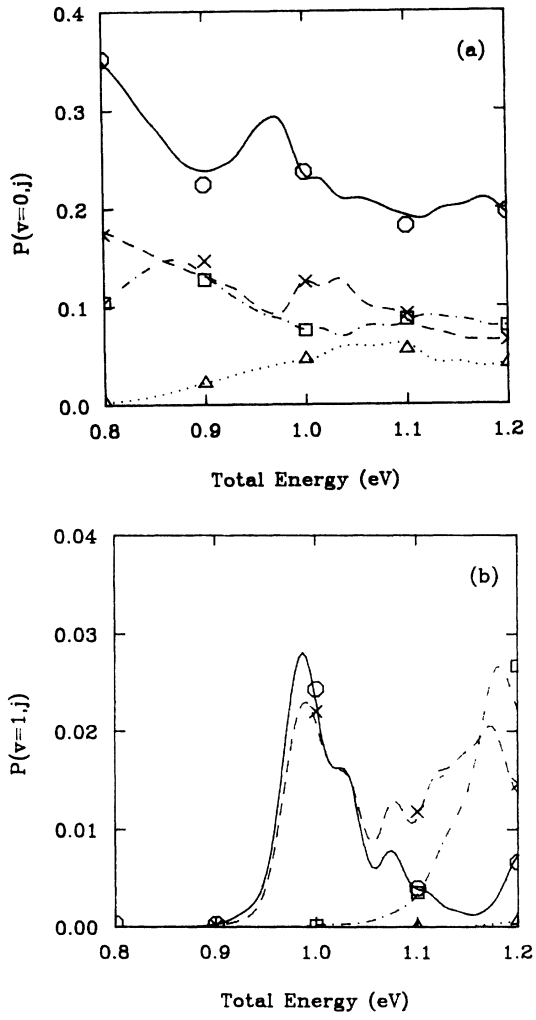

FIG. 4. (a) Rotationally resolved inelastic probabilities for $v=0$, $P_{in}(v_0,j_0 \rightarrow v=0,j|E)$. The different j states are indicated as follows: ($j=0$), ——, ○; ($j=2$), — — —, ×'s; ($j=4$), —·—·—·, □; ($j=6$), · · · ·, △. The continuous curves give the results of the present calculation and the symbols give the results from Ref. 2(b). (b) The same as in 4(a), except for $v=1$.

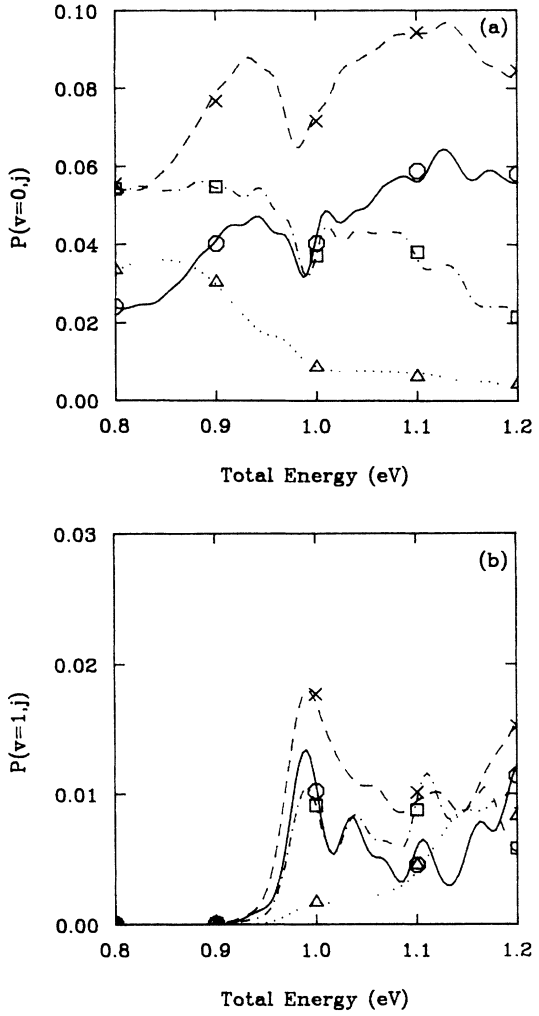

FIG. 5. (a) Rotationally resolved reactive probabilities for $v=0$, $P_r(v_0,j_0\rightarrow v=0,j|E)$. The symbols are the same as in Fig. 4. (b) The same as in 5(a), except for $v=1$.

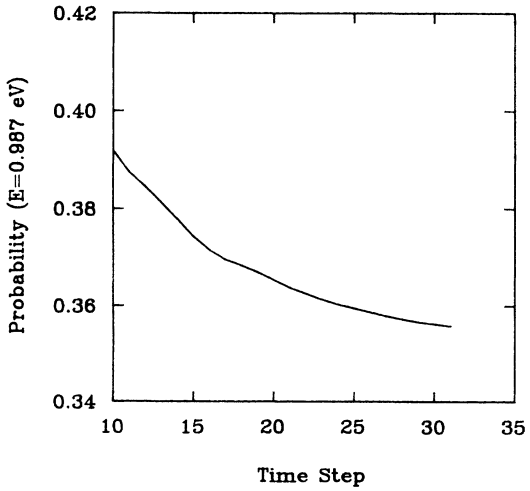

FIG. 6. An illustration of the convergence in time of the $v=0$ reactive probability, $P_r(v_0,j_0\rightarrow v=0|E)$, at the bottom of the 0.987-eV resonance. A single time step equals 0.5×10^{-14} sec, so, e.g., a total of 1×10^{-13} sec has elapsed by time step 20.

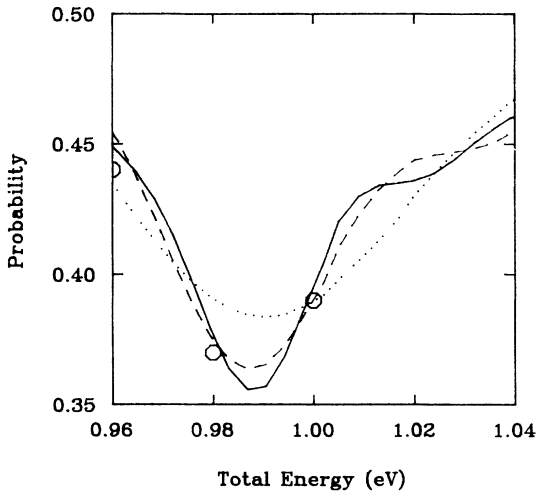

FIG. 7. An illustration of the shape of the 0.987-eV resonance as a function of time. The dotted curve is for time step 11, the dashed curve for step 21, and the solid curve for step 31.

effort involved as it gives an upper limit on what will be needed for similar calculations with an optimized code. A typical inelastic propagation took approximately 5500 s on a Cray-2 (NASA-Ames) and the corresponding reactive propagation took 7500 s. These two calculations yield the S-matrix elements out of a single initial state at any energy in the range from 0.8 to 1.2 eV. Most of the CPU time is used in calculating the action of the Hamiltonian on the wave function in the Chebyshev propagation method. The numbers of terms in the Chebyshev expansion of the propagator were about 6500 and 7000 for the inelastic and reactive runs, respectively. Note that the number of expansion terms is more or less fixed and that efforts at optimization should be directed at decreasing the cost of the action of the Hamiltonian operator. Substantial reductions can be achieved by making use of the fact that outside the strong interaction zone, greatly reduced numbers of vibrational and rotational states are required compared to the numbers used inside the strong interaction region. As discussed in Sec. V, this means that the close-coupling wave-packet (CCWP) method can be used in the outer regions, leaving only a wave-packet propagation in one variable. Due to the decreased coupling in this region, the matrix Hamiltonian is small enough to reduce the effort of applying the Hamiltonian.

V. DISCUSSION

In this paper we have developed and demonstrated an alternative time-dependent method for efficiently performing three-dimensional reactive scattering calculations. As the problem size grows, our scheme should become even more efficient due to the slow scaling of wave-packet methods. Even now, we are able to perform purely inelastic calculations on heavy systems such as $O+N_2$ ($J=0$).[48] We are also examining a number of modifications to our technique that should make it even more efficient. The projection operator approach[30] can be combined with the methods of this paper to allow us to reduce the size of the (R,r) grids we currently use,

thereby decreasing the propagation cost. It is also possible to perform the final-state analysis by Fourier analyzing the wave function in time at one point in R (which could be placed just as the interaction potential goes to zero) as opposed to integrating over space at one point in time.[31,32] This would allow us to cut off the reactive grid at very short distances. If one only desires vibrationally resolved probabilities, it is possible to move the analysis point in further yet. Every decrease that can be made in the size of the space grids needed for performing the propagation yields a corresponding decrease in the cost of the propagation. The rotational close-coupling body-frame formalism we currently use scales as $N^{3/2}$, where N is the number of (j,Ω) states. By explicitly propagating in the γ variables, the overall scaling can be reduced to $N \ln N$. This modification is currently being tested for inelastic scattering.[49] It is also possible to use other propagation techniques that could in principle be faster than the Chebyshev-FFT method used here. It has been hoped for a number of years that time-dependent wave-packet methods would provide a practical alternative to the costly time-independent methods for performing reactive scattering calculations, and we believe that methods such as ours will soon fulfill these hopes.

ACKNOWLEDGMENTS

One of us (D.J.K.) gratefully acknowledges helpful conversations with Professor R. Kosloff of the Hebrew University. The authors gratefully acknowledge partial support of this research under NASA-Ames Research Center Grant No. NAG 2-503 and by the Texas Advanced Research Projects, Texas Higher Education Coordinating Board.

[1]A. Kuppermann and P. G. Hipes, J. Chem. Phys. **84**, 5962 (1986); P. G. Hipes and A. Kuppermann, Chem. Phys. Lett. **133**, 1 (1987).

[2](a) K. Haug, D. W. Schwenke, Y. Shima, D. G. Truhlar, J. Z. H. Zhang, and D. J. Kouri, J. Phys. Chem. **90**, 6757 (1986); (b) J. Z. H. Zhang, D. J. Kouri, K. Haug, D. W. Schwenke, Y. Shima, and D. G. Truhlar, J. Chem. Phys. **88**, 2492 (1988).

[3]F. Webster and J. C. Light, J. Chem. Phys. **85**, 4744 (1986); **90**, 265 (1989); **90**, 300 (1989).

[4]D. W. Schwenke, K. Haug, D. G. Truhlar, Y. Sun, J. Z. H. Zhang, and D. J. Kouri, J. Phys. Chem. **91**, 6080 (1987); D. W. Schwenke, K. Haug, M. Zhao, D. G. Truhlar, Y. Sun, J. Z. H. Zhang, and D. J. Kouri, *ibid.* **92**, 3202 (1988).

[5]J. Linderberg and B. Vessel, Int. J. Quantum Chem. **31**, 65 (1987); (unpublished).

[6]G. A. Parker, R. T Pack, B. J. Archer, and R. B. Walker, Chem. Phys. Lett. **137**, 564 (1987); R. T Pack and G. A. Parker, J. Chem. Phys. **87**, 3888 (1987).

[7]M. Baer and Y. Shima, Phys. Rev. A **35**, 5252 (1987); M. Baer, J. Phys. Chem. **91**, 5846 (1987); J. Chem. Phys. **90**, 3043 (1989).

[8]J. Z. H. Zhang and W. H. Miller, Chem. Phys. Lett. **140**, 329 (1987); J. Chem. Phys. **88**, 449 (1988).

[9]J. M. Launay and D. Lepetite, Chem. Phys. Lett. **144**, 346 (1988).

[10]D. Manolopoulos and R. E. Wyatt, Chem. Phys. Lett. **152**, 23 (1988).

[11]G. C. Schatz, Chem. Phys. Lett. **150**, 92 (1988); **151**, 409 (1988).

[12]J. Mazur and R. J. Rubin, J. Chem. Phys. **31**, 1395 (1959).

[13]E. A. McCullough and R. E. Wyatt, J. Chem. Phys. **54**, 3578 (1971); **54**, 3592 (1971).

[14]Ch. Zubert, T. Kamal, and L. Zulike, Chem. Phys. Lett. **36**, 396 (1975).

[15]E. Kellerhals, N. Sathymurthy, and L. M. Raff, J. Chem. Phys. **64**, 818 (1976); P. M. Agarwal and L. M. Raff, *ibid.* **74**, 5076 (1981).

[16]E. J. Heller, J. Chem. Phys. **68**, 3891 (1978); D. Huber and E. J. Heller, *ibid.* **87**, 5302 (1987); **89**, 4752 (1988); D. Huber, E. J. Heller, and R. G. Littlejohn, *ibid.* **87**, 5302 (1987); D. Huber, S. Ling, D. G. Imre, and E. J. Heller, *ibid.* **90**, 7317 (1989).

[17]K. C. Kulander, J. Chem. Phys. **69**, 5064 (1978); J. C. Gray, G. A. Fraser, D. G. Truhlar, and K. C. Kulander, *ibid.* **73**, 5726 (1980); A. E. Orel and K. C. Kulander, Chem. Phys. Lett. **146**, 428 (1988).

[18]R. Kosloff and D. Kosloff, J. Chem. Phys. **79**, 1823 (1983); J. Comput. Phys. **52**, 35 (1983); H. Tal-Ezer and R. Kosloff, J. Chem. Phys. **81**, 3967 (1984).

[19]M. D. Feit and J. A. Fleck, J. Chem. Phys. **79**, 301 (1983).

[20]C. Leforestier, Chem. Phys. **87**, 241 (1984); in *Theory of Chemical Reaction Dynamics*, edited by D. C. Clary (Reidel, Dordrecht, 1986), pp. 235–246.

[21]S. Sawada, R. Heather, B. Jackson, and H. Metiu, J. Chem. Phys. **83**, 3009 (1985); B. Jackson and H. Metiu, *ibid.* **85**, 4192 (1986); **86**, 1026 (1987); R. Heather and H. Metiu, *ibid.* **86**, 5009 (1987).

[22]Z. H. Zhang and D. J. Kouri, Phys. Rev. A **34**, 2687 (1986).

[23]R. C. Mowrey and D. J. Kouri, J. Chem. Phys. **84**, 6466 (1986); Y. Sun, R. C. Mowrey, and D. J. Kouri, *ibid.* **87**, 339 (1987); Y. Sun and D. J. Kouri, *ibid.* **89**, 2958 (1988).

[24]T. Joseph and J. Manz, Mol. Phys. **58**, 1149 (1986).

[25]S. Thareja and N. Sathymurthy, J. Phys. Chem. **91**, 1970 (1987).

[26]V. Mohan and N. Sathymurthy, Comput. Phys. Rep. **7**, 213 (1988).

[27]Y. Sun, R. S. Judson, and D. J. Kouri, J. Chem. Phys. **90**, 241 (1989).

[28]D. Neuhauser and M. Baer, J. Chem. Phys. **90**, 4351 (1989).

[29]D. Neuhauser and M. Baer, J. Chem. Phys. **93**, 2862 (1989).

[30]D. Neuhauser and M. Baer, J. Chem. Phys. **91**, 4651 (1989).

[31]D. Neuhauer, M. Baer, R. S. Judson, and D. J. Kouri, J. Chem. Phys. **90**, 5882 (1989); (unpublished).

[32]D. Neuhauser, M. Baer, R. S. Judson, and D. J. Kouri (unpublished).

[33]See, e.g., Comp. Phys. Commun. **53**, Nos. 1–3 (1989).

[34]R. T Pack, J. Chem. Phys. **60**, 633 (1974); P. McGuire and D. J. Kouri, *ibid.* **60**, 2466 (1974), and references therein.

[35]M. Tamir and M. Shapiro, Chem. Phys. Lett. **31**, 166 (1975).

[36]D. J. Kouri, T. G. Heil, and Y. Shimoni, J. Chem. Phys. **65**, 226 (1976).

[37]A. Kuppermann and G. C. Schatz, J. Chem. Phys. **62**, 2502 (1975).

[38]A. B. Elkowitz and R. E. Wyatt, J. Chem. Phys. **63**, 702

(1975).
[39]R. B. Walker and J. C. Light, Chem. Phys. **7**, 84 (1975).
[40]D. A. Micha, Ark. Fyz. **30**, 411 (1965); W. H. Miller, J. Chem. Phys. **50**, 407 (1969); see also G. H. Raiwitcher, Phys. Lett. **21**, 444 (1966); M. J. Seaton, Philos. Trans. R. Soc. London, Ser. A **245**, 469 (1953); D. W. Schwenke, D. G. Truhlar, and D. J. Kouri, J. Chem. Phys. **86**, 2772 (1987).
[41]D. M. Brink and G. R. Satchler, *Angular Momentum* (Oxford University Press, Oxford, 1971).
[42]*Handbook of Mathematical Functions,* Natl. Bur. Stand. Appl. Math. Ser. No. 55, edited by M. Abramowitz and I. A. Stegun (U.S. GPO, Washington, D.C., 1965).
[43]Pioneering work on this problem was due to J. O. Hirschfelder and E. P. Wigner, Proc. Nat. Acad. Sci. (U.S.A) **21**, 113 (1935). Later studies include those by C. F. Curtiss, J. O. Hirschfelder, and F. T. Adler, J. Chem. Phys. **18**, 1638 (1950); C. F. Curtiss, *ibid.* **21**, 1199 (1953); D. J. Kouri and C. F. Curtiss, *ibid.* **44**, 2120 (1966); W. R. Thorson, *ibid.* **42**, 3878 (1965); R. T Pack and J. O. Hirschfelder, *ibid.* **49**, 4009 (1968); K. P. Lawley and J. Ross, *ibid.* **43**, 2930 (1965); **43**, 2943 (1965).
[44]W. H. Miller, J. Chem. Phys. **50**, 407 (1969).
[45]R. Bisseling, Ph.D. thesis, Hebrew University, 1985.
[46]The literature on transition-state theory is enormous. A tiny sampling is as follows: P. Pechukas, in *Modern Theoretical Chemistry,* edited by W. H. Miller (Plenum, New York, 1970), Part B, Vol. 2, p. 285ff; Annu. Rev. Phys. Chem. **32**, 159 (1981); D. G. Truhlar, W. L. Hase, and J. T. Hynes, J. Phys. Chem. **87**, 2665 (1983); W. H. Miller, J. Chem. Phys. **65**, 2216 (1976); E. Pollak and P. Pechukas, *ibid.* **70**, 3256 (1979); in *Theory of Chemical Reaction Dynamics,* edited by D. C. Clary (Reidel, Dordrecht, 1986), pp. 135–165; B. C. Garrett and D. G. Truhlar, J. Phys. Chem. **83**, 1052 (1979); **83**, 3058(E) (1979); M. Baer, Chem. Phys. **123**, 365 (1988).
[47]B. Liu, J. Chem. Phys. **58**, 1925 (1973); P. Siegbahn and B. Liu, *ibid.* **68**, 2457 (1978); D. G. Truhlar and C. J. Horowitz, *ibid.* **68**, 2466 (1978); **71**, 1514(E) (1979); B. R. Johnson, *ibid.* **74**, 754 (1981).
[48]R. S. Judson, C.-K. Zhang, D. J. Kouri, and R. L. Jaffe (unpublished).
[49]C.-H. Yu, R. S. Judson, D. J. Kouri, and R. C Mowrey (unpublished).